

Low Cost, High Precision, Autonomous Measurement of Trunk Diameter based on Computer Vision.

Medición Autónoma de Diámetro de Tronco de Bajo Costo y Alta Precisión basado en Visión Computacional.

Diego Sebastián Pérez ¹, Facundo Bromberg ², Francisco Gonzalez Antivilo ³

¹ Laboratorio de Inteligencia Artificial DHARMA. Dpto. de Sistemas de la Información, UTN Regional Mendoza. Rodríguez 273, CP 5500, Mendoza, Argentina. sebastian.perez@frm.utn.edu.ar

² CONICET – Laboratorio de Inteligencia Artificial DHARMA. Dpto. de Sistemas de la Información, UTN Regional Mendoza. Rodríguez 273, CP 5500, Mendoza, Argentina. fbromberg@frm.utn.edu.ar

³ CONICET – Laboratorio de Fisiología Vegetal. Facultad de Ciencias Agrarias, Universidad Nacional de Cuyo. Alte. Brown 500, CP 5664, Chacras de Coria, Luján de Cuyo, Mendoza, Argentina. fgonzalezantivilo@gmail.com

ABSTRACT

Trunk diameter is a variable of agricultural interest, used mainly in the prediction of fruit trees production. It is correlated with leaf area and biomass of trees, and consequently gives a good estimate of potential production of the plants. This work presents a *low cost, high precision* method for *autonomous* measurement of trunk diameter of fruit trees based on *Computer Vision*. Autonomous methods based on Computer Vision or other techniques are introduced in the literature for they present important simplifications in the measurement process, requiring little to none human decision making. This presents different advantages for crop management: the method is amenable to be operated by unknowledgeable personnel, with lower operational costs; it results in lower stress levels to knowledgeable personnel, avoiding the deterioration of the measurement quality over time; or it makes the measurement process amenable to be embedded in larger autonomous systems, allowing more measurement to be taken with equivalent costs. In a more personal aspect, the present work is also a successful proof-of-concept for our laboratories and regional research institutions in favor of autonomous measurements based on Computer Vision, opening the door to further investigations in other important agronomic variables measurable by Computer Vision. To date, all existing autonomous methods are either of low precision, or have a prohibitive cost for massive agricultural adoption, leaving the manual Vernier caliper or tape measure as the only choice in most situations. In this work we present an autonomous solution that is costly effective for mass adoption, and its precision is competitive (with slight improvements) over the caliper method.

RESUMEN

El diámetro del tronco es una variable de interés agrícola utilizada principalmente en la estimación de la producción de árboles frutales. Se correlaciona con el área foliar y la biomasa de los árboles, y por lo tanto da una buena estimación del potencial productivo de las plantas. En este trabajo se presenta un método de bajo costo y alta precisión para la medición autónoma de diámetro de tronco de árboles frutales basado en técnicas de Visión Computacional. Se presentan algunos métodos autónomos existentes en la literatura, basados en Visión Computacional y otras técnicas, que logran simplificaciones importantes en el proceso de medición, requiriendo poca o ninguna intervención humana. La automatización presenta diferentes ventajas para el manejo del cultivo: es susceptible de ser utilizado por personal con poco o nulo conocimiento, llevando a costos operativos más bajos; requiere un menor nivel de estrés a personal con conocimientos, evitando el deterioro de la calidad de la medición a lo largo del tiempo; y hace que el proceso de medición sea susceptible de ser embebido en sistemas autónomos no tripulados, lo que permitiría realizar más mediciones con costos equivalentes. En un aspecto más personal, el presente trabajo resulta una prueba de concepto exitosa para nuestros laboratorios e instituciones de investigación regional en favor de mediciones autónomas, basadas en Visión Computacional, abriendo la puerta a nuevas investigaciones para otras variables agronómicas importantes, susceptibles de ser medidas mediante técnicas de Visión Computacional. Hasta la fecha, todos los métodos autónomos existentes son de baja precisión o tienen un costo prohibitivo para la adopción masiva en agricultura, dejando el calibre

de Vernier o la cinta métrica como la única opción en la mayoría de las situaciones. En este trabajo se presenta una solución autónoma, de bajo costo permitiendo la adopción masiva, y su precisión es competitiva (con leves mejoras) frente al método del calibre.

KEYWORDS: Trunk Diameter, Computer Vision, Autonomous Measurement, Physiology Measurements, Fruit Crop, Precision Agriculture.

PALABRAS CLAVES: Diámetro de tronco, Visión Computacional, Medición Autónoma, Mediciones Fisiológicas, Cultivo Frutícola, Agricultura de Precisión.

INTRODUCTION

The main contribution of this work consists in a *low cost, high precision and autonomous* measuring method of trunk diameter based on techniques for *Image Segmentation* of Computer Vision. Trunk diameter is a variable of agricultural interest in the production of fruit trees. The trunk of a plant complies with the vital function of transporting water and nutrients from roots to consumption areas (shoots, leaves, fruits), as well as with the accumulation of reserve substances (32). It is correlated with the capacity of the plant to sustain growth and maturation of shoots, leaves and fruits, and it is a good estimator of other indicators of the plant productive potential, such as biomass and leaf area (11, 12, 39). There are numerous allometric relationships reported estimating leaf area and biomass of different trees using mainly the cross-sectional diameter or area of the trunk (3, 10, 17, 24, 30, 40, 52). Therefore, obtaining accurate measurements of trunk diameter helps obtaining better estimates of variables such as leaf area and biomass, and consequently better estimation of potential production of the plants and the plants status evolution.

Table 1. Potential errors that can occur in the measurement process based on caliper.

Tabla 1. Errores potenciales que pueden ocurrir en el proceso de medición basado en calibre.

| ID | Error description |
|-----|---|
| I | Reading of the measuring instrument. |
| II | Transcribing values into the datasheet. |
| III | Writing values in the slot corresponding to its plant ID. |
| IV | Transcribing the datasheet into the computer. |
| V | Interpolation errors |

In practice, the trunk diameter is measured using manual methods such as Vernier calipers or measuring tapes. Although these instruments can be considered high precision (0.05mm in the case of a standard caliper and 0.5mm in the case of a standard tape), they may result in important measurement errors. On one hand there are the human errors that may occur during extensive measurement campaigns due to fatigue, haste or carelessness (errors I through IV in Table 1). Other errors may arise indirectly due to the elevated costs in labor stipends of the manual method that force agronomists to save in the number of trees for which measurements are performed. In practice, this may be mitigated using interpolation methods such as Krigging (16), but in practice even the minimal number of measurements required by these methods for accurate estimates may be prohibitive. We refer to this as *interpolation errors* and list it together with the other errors in Table 1. Without precise information of agronomic variables such as trunk diameter, agronomists may lack information required for selective harvesting (8), or proper and assertive decisions over crop management such as amount of watering, fertilizers and pruning (15); resulting not only in poor harvest predictions but in an unnecessary stress of the plant that may affect the fruit quality, production or even the life of plant.

Different autonomous measurement methods have been introduced in the literature with the hope of mitigating these errors. Mostly, their intent is not so much in increasing the precision of individual measurements, as manual methods already present sufficient precision, but more on mitigating the effect of manual or interpolation errors due to human fatigue or elevated costs of human labor. An autonomous system reduces to a minimum the required human intervention during the measurement process. Our method, although not entirely autonomous as it requires taking a

photograph and fixing a quick clamp manually, it requires little to none knowledgeable decision making, which makes it possible to be operated by unknowledgeable, and thus lower stipend or more available personnel. Also, it opens the possibility of further automation by embedding the system within a mobile system that autonomously measures large number of trees (e.g., unmanned land or air vehicles). Such a system would allow massive measurements of the entire population of trees, with the consequent benefits in crop management operations. This is the goal of *Precision Agriculture* (PA) that has been the response of the scientific and industrial community for mitigating the impact of interpolation errors. As a whole, the PA is a group of technologies that increase the spatial resolution of crop management by providing the means to reduce the costs of measurements and interventions, thus increasing the spatial density of the treatments. Among its technologies we can list autonomous sensors embedded in wireless ad-hoc sensor networks, GPS systems for global positioning, geographical information systems for proper management of the sensed data, autonomous systems for differential management of the inputs, and other technologies of information and computation (6). Recent years has shown an important increase in the adoption of these technologies both in production and academic settings. Examples for wheat, soy, potato, corn, beet, barley, sorghum, cotton, oats, and rice can be found in (6), together with important advances in the commercial application of PA for the production of vineyards (2, 7), citric trees (45), banana trees, tea, date palm trees, and even management of sport fields (5) and train systems (1). In parallel, several Universities and research groups around the world raised their academic interest in PA as exemplified by the *International Conference on Precision Agriculture* being held continuously since 1990, together with the *European Conference on Precision Agriculture* that has been held in nine occasions since 1996. In addition, many aspects and contributions of PA have been discussed regularly in general agricultural meetings and journals.

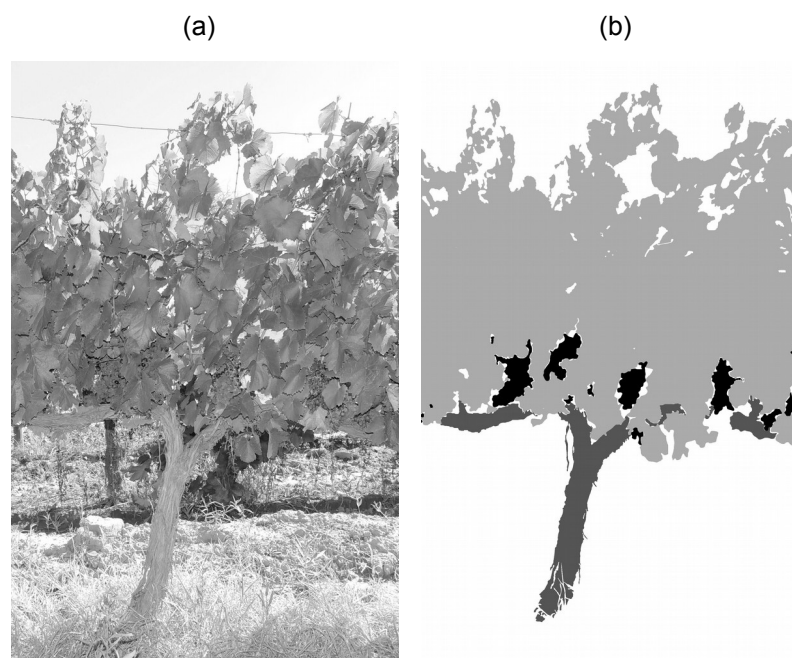


Figure 1. (a) Original image of a grape vine. (b) Segmentation into four regions: grape (black), trunk (dark grey), foliage (light grey), and the rest of the scene named *background* (white).

Figura 1. (a) Imagen original de una vid. (b) Segmentación en 4 regiones: uva (negro), tronco (gris oscuro), follaje (gris claro), y el resto de la escena llamado *background* (blanco).

The advantages and benefits provided by the PA are sustained mainly by the technologies of autonomous sensing. The market presents autonomous sensors for a great diversity of magnitudes such as temperature, humidity (air and soil), luminosity, solar radiation both visible and ultraviolet spectrum, different gases, atmospheric pressure, NDVI, and more. However, some magnitudes are too complex for existing electronic sensors that still require human visual inspection. Such is the case of trunk diameter, fruit grain diameter, leaf area, bud count, fruit localization within trees, defects in fruit surface, weed localization, optimal harvesting time, among others. All these (and other) variables are strongly correlated with quality and productive potential of the crop but are currently mostly

excluded from the reach of PA. Motivated by this situation, is that in 2012 we begun a collaboration between the *DHARMA Laboratory on Artificial Intelligence* (National Technological University, Mendoza Regional Faculty) and the *Plant Physiology Laboratory* (Faculty of Agricultural Sciences, National University of Cuyo), to contribute with *Computer Vision* techniques applied to autonomous sensing of complex agricultural magnitudes, starting with the autonomous measurement of trunk diameter presented in this paper. Other contributions exists in the area, such as: differential fumigation (42, 49), fruits localization in trees (21, 25), fruit surface defects detection (27), weed identification and control (19, 26, 33, 47), verification of NDVI (37), estimation of fruit diameter (53), optimum harvesting timing (44, 54), and more (14, 35).

Our contribution takes advantage of *Image Processing* and *Image Segmentation* techniques, which are supported by advances in fundamental algorithms of *Computer Vision* such as *Markov Random Fields*, *Conditional Random Fields*, *Edge Detection*, *Clustering*, *Fuzzy Sets*, *Thresholding*, *Texture analysis*, *Deformable Models*, among others (4, 48). *Image Processing* is the use of computer methods for preprocessing a digital image and converts it into a form suitable for further analysis (48). The term *Image Segmentation* refers to the process of partitioning a digital image into a set of regions, each of which is strongly correlated with some object of the real world, or background. The pixels of each region are grouped based on some uniformity criteria (see Appendix A). For instance, Figure 1-a shows the original image of a grape vine and Figure 1-b its segmentation into four regions: grape (black), trunk (dark grey), foliage (light grey), and the rest of the scene named background (white).

Previous works

Several works of autonomous measurement of trunk diameter has been presented previously in the literature. For instance, *Tetuko et al* (50) propose a method for estimating ranges of values of trunk diameters over large areas of dense forests of four species of Java-Indonesian trees. Their approach projects L-band microwaves on the trunks, and uses a Synthetic Aperture Radar (SAR) to read the resulting backscattering coefficient, later correlated with trunk diameter. In their paper they use a SAR mounted on the JERS-1 satellite, which has a resolution of *18mt* per pixel, although other existing SARs may range from *200mt* per pixel (low resolution) to *1mt* per pixel (high resolution). Technologies known as airborne SAR sensors (mounted on airplanes or other atmospheric aircrafts) achieve resolutions of *10cm* to *30cm* per pixel, but require specialized and expensive equipment. Satellite SARs, in contrast, require access to a satellite, with lower cost and higher availability than the airborne version, but still prohibitive or inaccessible to most producers. In either case, however, the resolutions are still large enough to prevent their use in any practical PA application. *Jutila et al* (22) presents a method designed for forest harvesters. Their method consists in a 2D laser range finder (of *SICK Sensor Intelligence* company) mounted on an all-terrain vehicle, used to obtain depth information. Their method achieves good precision in pines forests with an error mean of *0.6cm* and standard deviation of *2.2cm*. One limitation for adoption of this technique in fruit trees production is the high cost of equipment needed for implementation. In *Omasa et al* (41), a 3D model of a city park was used in order to quantify the biophysical variables of trees, such as height, canopy diameter and trunk diameter. The 3D model was generated with a scanning Light Detection and Ranging (LIDAR) technology, combining data from airborne sensors with data on-ground using portable sensors. The authors reported errors less than *0.3cm* in the three trees that were measured. While this method shows high precision, the high cost of aerial and portable LIDAR sensors makes it privative for most fruit trees producers. *Kan et al* (23) presented a method based on Computer Vision for measuring trunk and branch diameters from images acquired by a conventional digital camera. A calibration stick is included in the scene next to the tree trunk, and it is detected using template matching (9). The trunks and branches of the tree are also detected by template matching and then the number of trunk and branch pixels is counted. The actual diameters are obtained by multiplying the trunk and branch diameters in pixels by the size of a pixel obtained through the calibration stick. This method was tested on 50 images resulting in a mean error of *0.67cm* and standard deviation of *1.73cm*. However, when the background of the images is complex (for instance, not a clear sky), the calibration stick may not be detected and the method fails to obtain the diameters. The results over the 50 images show a success rate of 90% in detecting the calibration stick. For a definite assessment of their approach one would require information on the proportion of these images with complex backgrounds. This information is not reported however. *Thamrim et al* (51) discussed a new and relatively simple tree diameter measurement technique using a high-performance, non-intrusive infrared sensor. The experiments were conducted in a controlled laboratory environment under ambient light condition produced by a fluorescent lamp, with four cylindrical poles of different diameters used as controlled

replacements for trees. About 80% of the experiments show errors of less than 0.2cm for each pole, with an average of 0.2cm for standard deviations. The rest of the results give errors between 4cm to 5cm as a consequence of the extra complexity of their problem caused the sensor mounted on a moving vehicle. Although these results are promising, they still present 20% of cases with unacceptable errors on a controlled environment.

Our Contribution

All the above techniques have significantly contributed in the process of obtaining a high precision, low cost autonomous measurement technique of fruit trees trunk diameter. However, these solutions are not optimal: some are low cost but low precision (or equivalently high failing rate), and others are high precision but high cost. In this paper we propose a *low cost, high precision* method based on *Computer Vision* for autonomous measurement of trunk diameter of fruit trees, whose cost is in the order of Kan's technique (the lowest of all) and whose precision is in the order of Omasa's (the highest of all). Equivalently, our approach presents precision equivalent to a Vernier caliper with a larger but still accessible cost (the digital camera, a PC and the quick clamp whose value ranges in the 30 US dollars), while maintaining the advantage of automation.

Our method consists in digitally processing images of a quick clamp (see Figure 2-a) gripped to the trunk (see Figure 2-b), obtained with standard commercial digital camera on realistic conditions of climate and luminosity. The images are computationally processed using the Computer Vision technique called *image segmentation* that discriminates the pixels of the clamp from the rest of the image, as illustrated in Figure 2-c. The measurement is completed by first measuring the horizontal distance in pixels between the internal edges of the clamps, and converted to centimeters multiplying this distance to the distance in centimeters of a pixel; obtained from the previously known height of the clamps in centimeters and its measure in pixels. In addition to a known height, the clamp also serves the purpose of determining the preferred location of the trunk diameter measurement. These stages of the method are presented in more detail in the following section. In personal conversations with agronomists, they considered our approach extremely simple, even simpler than measuring using a Vernier caliper. However, we present no proof in favor of this argument, leaving it for personal consideration of the reader.

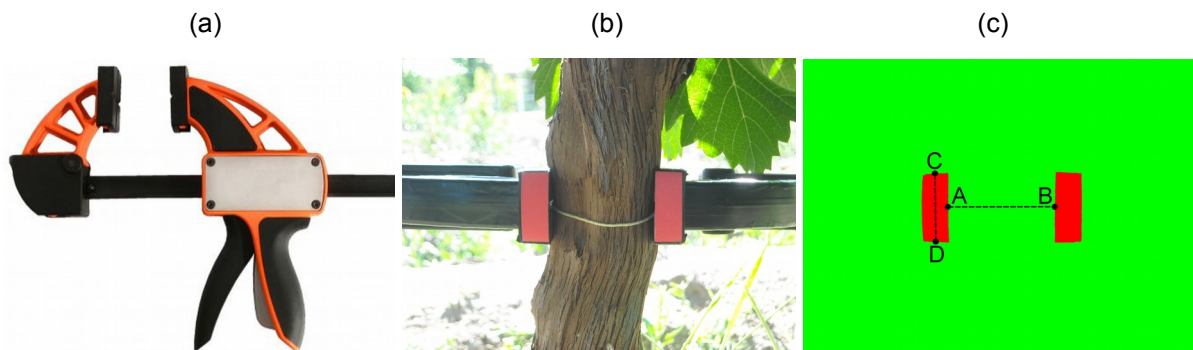


Figure 2. (a) Quick clamp. (b) Original Image with the quick clamp. (c) Results obtained by the GMM segmentation algorithm for the original image and calculating the distance in pixels between the spade pads (points A-B) and height in pixels of a spade pad (C-D points).

Figura 2. (a) Pinza rápida. (b) Imagen original con la pinza rápida colocada. (c) Resultado obtenido por el algoritmo de segmentación GMM para la imagen original, y cálculo de la distancia en píxeles entre los tacos de la pinza (puntos A-B) y altura en píxeles de un taco (puntos C-D).

The viability of this approach was assessed by comparing its results with the manual method based on caliper. The results show that the autonomous approach obtains a mean absolute error of 1.05mm and a standard deviation of 0.95mm , resulting trunk diameter values equivalent (slightly better) than to those of the manual method (see Table 2). In addition, our method presents two clear advantages over the manual method: avoids errors I, II, and IV (see Table 2); and eliminates the operator qualifications as an influencing factor, i.e., requires people with little or null knowledge and experience in agronomic experiments.

MATERIALS AND METHODS

This section describes the implementation details of our autonomous image-based method, as well as details on the experimental setups used for evaluation.

A. Implementation of Autonomous Image-based Method (AIM)

Trunk diameter measurements using image processing presents several difficulties. First, the trunk must be segmented out from the other elements of the scene such as soil, leaves, fruits, sky, and other plants. Second, the direction of the measurement must be detected. Third, the preferred measurement position along the trunk must be detected. Fourth, it is necessary to measure the distance in pixels between the edges of the trunk in the direction of measurement just determined. And conclude by re-scaling the measurement from pixels to millimeters.

In this work we incorporate the use of a modified quick clamp (shown in Figure 2-a) to address all these difficulties. The segmentation problem is simplified by changing the color of the spade pads of the grip to red as illustrated in Figure 2-b, a color rarely encountered in vineyards. With this modification it is possible to use simple color segmentation techniques for a successful and precise segmentation of the spade pads. With the spade pads segmented as illustrated in Figure 2-c, all remaining difficulties are easily addressed. The vertical of the pads is used as the direction of measurement, the position of the clamp along the trunk determines the preferred position for measurement, and the distance between their internal edges (points A and B in Figure 2-c) matches exactly the trunk diameter. Finally, the known height of the spade pads in millimeters $|C-D|_{mm}$ and in pixels $|C-D|_{pixels}$, obtained for the segment CD in the Figure 2-c, serves as a re-scaling ratio for converting the diameter $|A-B|_{pixels}$ in pixels to the diameter $|A-B|_{mm}$ in millimeters as follows:

$$|A-B|_{mm} = \frac{|C-D|_{mm}}{|C-D|_{pixels}} |A-B|_{pixels} \quad (1).$$

In practice, however, possible segmentation errors were averaged out by measuring several points A_n and B_n to obtain the reported diameter value:

$$|A-B|_{pixels} = \frac{1}{N} \sum_{n=1}^N |A_n - B_n| \quad (2).$$

With this setting, the measurement process requires the personnel to fix the clamp in the trunk, take the picture, and run it through our algorithm.

The spade pads segmentation technique consists in two stages: *training* and *classification*. The training stage uses manually segmented images to estimate a probabilistic model from color and segment information of pixels to later, during the classification stage, use the model to segment images autonomously by deciding the most probable segment of each pixel, given its color. Let us first introduce the details of the probabilistic model class we used: *Gaussian Mixture Models* (GMM) (4, 53), to later explain in detail the training and classification stages. GMMs are a weighted sum of Gaussian distributions that provide a multi-modal class of multi-variate density models. Figure 3-a shows an example for three Gaussians, colored red, green and blue; where each one has been already re-scaled by its weight. The figure also shows in black the resulting GMM. These models have two important advantages that make them particularly convenient for color image segmentation, as exemplified by the works (4), (18), and (48). On one hand, they have strong representational power, that by using a sufficient number of Gaussians, and by adjusting their means and covariances as well as the weights in the sum, almost any density can be approximated to arbitrary accuracy (4). On other hand, there are well-known, computationally efficient techniques for parameters estimation. In this work we used for parameter estimation the elegant and powerful method of *maximum likelihood* executed with the *Expectation-Maximization* algorithm (36). The works in (4, 18) explain in detail how to combine maximum likelihood in the algorithm Expectation-Maximization algorithm for estimating the numerical parameters of the GMM (i.e., means, covariance matrixes, and weights).

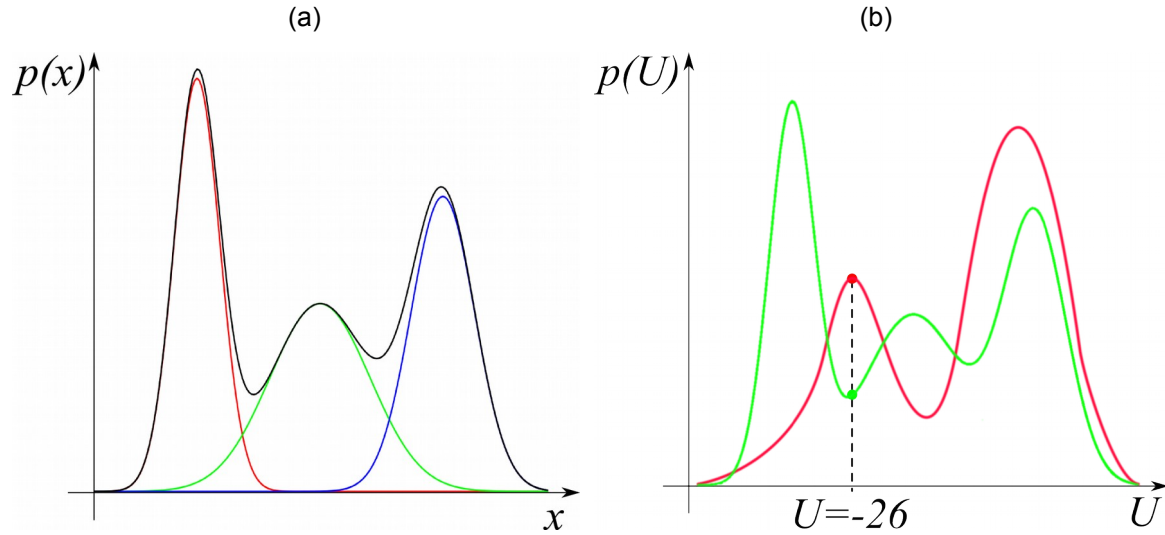


Figure 3. (a) Distribution modeled as a GMM (black line) with three Gaussians, red, green and blue lines, with weights already incorporated. (b) GMMs learned during training for the spade pads (red curve) and background (green curve). Only the dimension U is shown.

Figura 3. (a) Distribución modelada como una GMM (línea negra) con tres Gaussianas, líneas roja, verde y azul, con sus pesos ya incorporados. (b) GMMs aprendidas durante el entrenamiento para los tacos de la pinza (rojo) y el *background* (verde). Solo se muestra la dimensión U .



Figure 4. Images used as training data to model the GMMs. Top, images taken during a sunny day. Bottom, pictures taken on a cloudy day.

Figura 4. Imágenes utilizadas como datos de entrenamiento para modelar las GMMs. Arriba, imágenes tomadas durante un día soleado. Abajo, imágenes tomadas en un día nublado.

Training stage. During the *training* stage, a set of manually segmented images are used to estimate a GMM distribution used to model the probability that a pixel belongs to certain segment or object in the image (e.g., foliage, trunk, fruit). This stage is conducted during the design of the algorithm using images that are representative of the realistic conditions that may occur later during the measurement stage. In this work we used the well mixed set of cloudy and sunny images shown in Figure 4. For training, these figures have been manually segmented into two segments: spade pads and background, as exemplified in Figure 5. The set of all pixels of all 8 images were separated into two datasets, one per segment; with each datapoint containing the color information of the pixel. Image color is commonly coded according to the RGB color-space, i.e., the color of each pixel is represented by 3 components: red (R), green (G), and blue (B). For instance, in Figure 5 we show two pixels α and β , one for each segment. The RGB color code for these pixels is $\alpha=(245, 75, 48)$ and $\beta=(71, 126, 76)$. Experience from previous works (45) show that segmentation can be improved when the images are converted to the *LUV* color-space (L =*luminescence*, U =*saturation*, V =*hue angle*), and

the luminosity component discarded, i.e., using only the saturation and hue angle components (13, 20, 48). Our datapoints, and therefore the resulting GMMs are 2D. For instance, converted to UV our two example datapoints become $\alpha=(135, 38)$ and $\beta=(-26, 31)$. We provide more details on color spaces in Appendix B. The two datasets (one per segment) consists therefore on the U and V values of each pixel corresponding to the segment of the dataset. Figure 6 illustrates this information as two, 2D scatter plots over the UV space, one for the pixels in the background (right), and one for the pixels of the spade pads (left). In addition, two histograms are shown for each plot, one for the U component (on the top horizontal side) and one for the V component (on the right vertical side). These histograms show empirically the multimodal nature of the background, and the unimodal nature of the spade pads. This justifies using a two modes GMM for modeling the spade pads color information, and at least a three modes GMM for modeling the background color information.

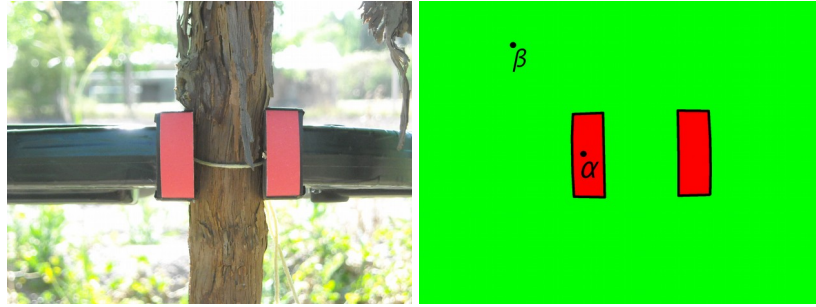


Figure 5. Left, original training image. Right, manually segmented image.

Figura 5. Derecha, imagen de entrenamiento original. Izquierda, imagen segmentada manualmente.

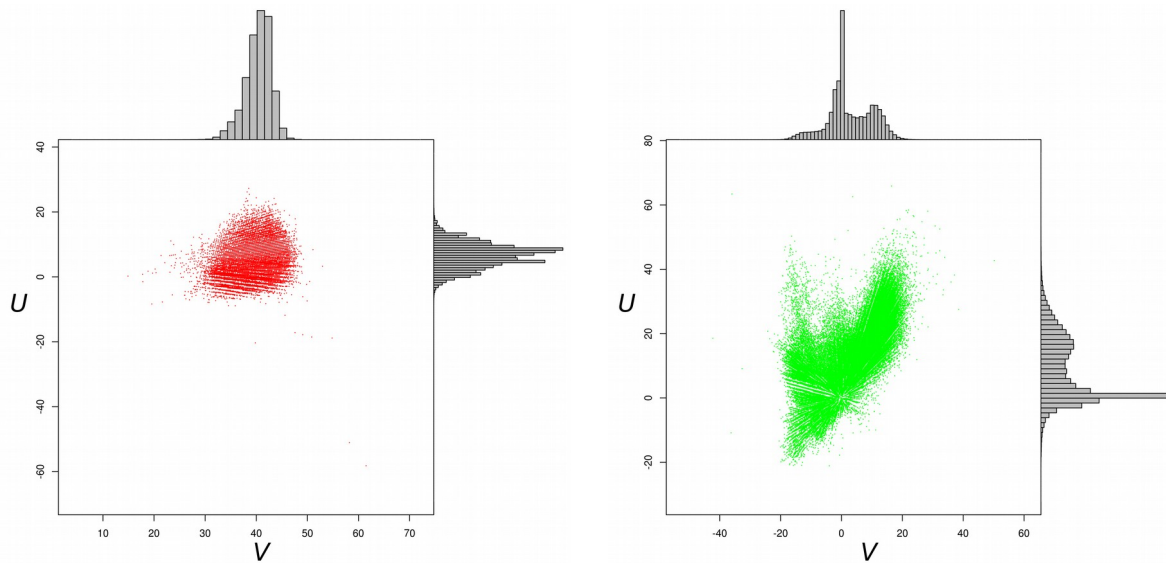


Figure 6. Scatter plot in the UV color-space for spade pads pixels (left) and the background pixels (right) of the image in Figure 2-d, together with the normalized histograms for U (top) and V (left) of each graph.

Figura 6. Diagrama de dispersión en el espacio de color UV para los píxeles de los tacos de la pinza (izquierda) y los píxeles del background (derecha) de la imagen de la Figura 2-d, junto a los histogramas normalizados de U (arriba) y V (izquierda) de cada gráfico.

We summarize the training stage as follows:

1. Take several pictures with the quick clamp attached to the trunk as shown in Figure 2-b on varying realistic conditions of climate and luminosity.
2. Convert all pictures to the LUV color space and discard the L component.

3. Using software for image editing, label all pixels in each image that correspond to the spade pads and background (for instance, coloring them red and green, respectively, as exemplified in Figure 5), and separate them into two datasets.
4. Using the training dataset of each segment, estimate the maximum likelihood numerical parameters of its corresponding GMM using the expectation-maximization algorithm.

Classification stage. During the measurement campaign, new images are autonomously segmented using the GMM models estimated previously during the training stage. This occurs in what is commonly called the *classification stage*, a stage that discriminates each pixels as part of the spade pads or as part of background. The classification decision is conducted using the GMMs learned during training for computing the probability that a pixel is part of the spade pads (using the spade pads GMM), or part of the background (using the background GMM). The pixel is assigned to the segment with highest probability. To illustrate, consider the two 1-dimensional GMMs shown in Figure 3-b in green and red. Assuming these GMMs were those learned during training for the spade pads (red curve) and background (green curve), the β point, with $U_\beta = -26$ as shown in the figure, would have a higher probability for the background GMM, and thus would be classified as background.

We summarize the classification stage as follows:

1. For the trunk to be segmented, fix the quick clamp to the trunk in the preferred position and take the picture (see Figure 2-b).
2. Convert the picture to the LUV color space and discard the L component.
3. Given the GMMs estimated during the training stage, run the classification subroutine to segment the image. This consists in determining the most probable segment for each pixel.
4. To obtain the trunk diameter, find the edge points A , B , C , and D as shown in Figure 2-c and average them out using Eq. (1) to obtain the diameter in pixels.
5. Re-scale the diameter in pixels to the diameter in millimeters using the computed height in pixels in Eq. (2).

B. Experimental setup

In this section we describe the experimental setup used for confirming our main claim: that our autonomous image-based method (AIM) for trunk diameter measurement produces results with precision equivalent to those obtained with the Vernier caliper method (CM), in realistic conditions of climate and luminosity, while maintaining the operational simplicity. The two methods are contrasted through their measurement errors. To obtain these errors we require the true value of the diameter. Although there may be several approaches for obtaining such value, we decided to use a non-standard, but nonetheless precise method: the *manual image-based method* (MIM), which matches exactly the AIM method with the exception that the segmentation is performed manually using standard image editing software with extreme care. This method therefore avoids errors produced by the autonomous segmentation method, only introducing rounding errors caused by the resolution of camera. Pixels in this work correspond to approximately 0.1mm, equivalent to the 0.05mm precision of a Vernier caliper. For the case of AIM this results in a very convenient error that measures the error of the segmentation. For the case of CM, this error highlights the potential manual errors I, II, or IV (c.f. Table 1) caused by a careless operator conscious or unconsciously, either due to some imperfection of his senses (potentially altered by the ambient context) or by his ability and experience in taking these type of manual measurements.

For a robust evaluation we compared the two methods over several images taken in realistic conditions of ambient luminosity (affected by climate) and different experiences of the operators, on real vineyards with vertical trellising system in the experimental fields of the *Plant Physiology Laboratory*, Faculty of Agricultural Sciences, National University of Cuyo (Lujan de Cuyo, Mendoza, Argentina). All the pictures were taken using a NIKON COOLPIX L16 compact commercial camera, in JPEG format with a resolution of 2048x1536 pixels (3 megapixels). For the caliper measurements we used a standard, plastic, Vernier caliper with precision of $0.5mm$. First the measurement of the diameter is done by manipulating the caliper to set the magnitude and then this result is recorded on notepads or paper forms. Later, information is loaded in computer spreadsheets for its posterior processing and analysis.

Operator experience experiment

In the first experiment the intent was to reproduce two realistic scenarios for our operators: inexperienced and experienced operators. The luminosity conditions were variable, taking all pictures under sunny and cloudy conditions. In the first case two operators were chosen that had no experience whatsoever on agronomic experiments but they were instructed to be extremely careful in their measurements (especially on the manual ones). The intent was to minimize the potential human error on these measurements, thus challenging the competitor AIM. The second case also consisted on two operators, but this time we chose two experienced graduate students of Agronomy Engineering of the *Faculty of Agricultural Sciences* that were hired and paid for their labor. This latter scenario was designed to reproduce the most common conditions under which the CM measurements are currently conducted in real-life. In both cases AIM was up to the challenge, resulting in lower errors as shown and discussed in the Results section.

For these experiments, each of the four operators conducted 7 rounds of caliper measurements (CM) over each of 30 grapevine plants, and 7 rounds of image-based measurements (AIM) over the same plants. This totaled 840 measurements per method, 210 per operator. The caliper and image measurements were taking on the same position of each plant's trunk on the position indicated by a previously positioned string as shown in Figure 2-b. Also, prior to the measurements, the bark was removed from each plant, around the target measurement position. By bark we refer to the rhytidome or dead tissue that forms around the trunk of a woody plant. In grapevine plants the bark is thick, rough and breaks off in longitudinal strips, and can represent up to 10% of the trunk diameter. By removing the bark, the observed variability in data corresponds only to the errors of Table 1.

Luminosity conditions experiment

In the second experiment the intent was to challenge our image-based method by imposing extreme solar luminosity conditions. Solar luminosity is strongly affected by climate conditions such as cloudy skies, which may change radically, even during the duration of a measuring campaign (see Figure 4). Intuitively, the experiment consisted in training the GMM model using *only* images of one condition type (e.g., sunny), and testing its performance by segmenting images taken during another luminosity condition (e.g., cloudy). Then, the diameters obtained were contrasted against those obtained by matching conditions, in our example segmentation of sunny images over the sunny model. Specifically, the experiment consisted in two sets of 20 images each, the *sunny set* taken during a sunny day, and the *cloudy set* taken during a cloudy day. From each set, a subgroup of 4 images was separated randomly and used for training the corresponding GMM models M_{cloudy} and M_{sunny} , leaving a total of 16 images on each set used later for testing the autonomous segmentation (denoted S_{sunny} and S_{cloudy} respectively). The two models and two 16 images sets were used in two crossed evaluations. One in which the 16 sunny images were segmented using the cloudy model, denoted $S_{sunny}|M_{cloudy}$, and another where the 16 cloudy images were segmented using the sunny model, denoted $S_{cloudy}|M_{sunny}$. To assess the precision of these segmentations, each case was contrasted against the case of matching conditions, i.e., the sunny set segmented against the sunny model (instead of the cloudy one), denoted $S_{sunny}|M_{sunny}$, and the cloudy set segmented over the cloudy model (instead of the sunny one), denoted $S_{cloudy}|M_{cloudy}$. In summary: $S_{sunny}|M_{cloudy}$ tested against $S_{sunny}|M_{sunny}$; and $S_{cloudy}|M_{sunny}$ tested against $S_{cloudy}|M_{cloudy}$.

RESULTS and DISCUSSION

This section reports and discusses the results obtained for our two experiments. In both cases we report some aggregation of the absolute errors $|AIM - MIM|$ and $|CM - MIM|$ of the AIM and CM methods, respectively.

Operator experience experiment

The results for the operator experience experiments are reported in Table 2. The table shows the mean and standard deviation (in parenthesis) of the absolute error over the 420 measurements of the inexperienced operator (top), and the 420 measurements of the experienced operators (bottom).

Table 2. Mean and standard deviation (SD) of the absolute error for the caliper-based method (CM) and the autonomous image-based method (AIM), reported for two use cases: inexperienced (top) and experienced (bottom) operators.

Tabla 2. Media y desviación estándar (SD) del error absoluto para el método basado en calibre (CM) y método autónomo basado en imágenes (AIM), reportado para dos casos de uso: operarios sin experiencia (arriba) y con experiencia (abajo).

| | | MEAN (SD) in cm |
|---------------|-----|-----------------|
| Inexperienced | CM | 0.132 (0.150) |
| | AIM | 0.101 (0.101) |
| Experienced | CM | 0.136 (0.139) |
| | AIM | 0.126 (0.097) |

Table 3. Results for the luminosity experiments shown in centimeters. Table (a) shows results comparing the two cloudy cases $S_{cloudy}|M_{sunny}$ vs. $S_{cloudy}|M_{cloudy}$ and Table (b) shows results for the two sunny cases $S_{sunny}|M_{cloudy}$ vs. $S_{sunny}|M_{sunny}$.

Tabla 3. Resultados para los experimentos de luminosidad mostrados en centímetros. La Tabla (a) muestra los resultados comparando los casos $S_{cloudy}|M_{sunny}$ vs $S_{cloudy}|M_{cloudy}$ y la Tabla (b) muestra los resultados para los dos casos $S_{sunny}|M_{cloudy}$ vs $S_{sunny}|M_{sunny}$.

| | 1 | 2 | 3 | 4 | 5 | 6 | 7 | 8 | 9 | 10 | 11 | 12 | 13 | 14 | 15 | 16 | | |
|-------------------------|-------|-------|-------|-------|-------|-------|-------|-------|-------|-------|-------|-------|-------|-------|-------|-------|------|----|
| $S_{cloudy} M_{cloudy}$ | 5.027 | 5.067 | 5.012 | 5.055 | 5.063 | 5.062 | 5.019 | 5.041 | 5.07 | 5.078 | 5.772 | 5.789 | 5.789 | 5.727 | 5.809 | 5.711 | Mean | SD |
| $S_{cloudy} M_{Sunny}$ | 5.021 | 4.982 | 4.973 | 5.021 | 5.032 | 5.033 | 4.996 | 5.017 | 4.989 | 5.035 | 5.685 | 5.731 | 5.702 | 5.698 | 5.747 | 5.669 | | |
| Difference | 0.006 | 0.085 | 0.039 | 0.034 | 0.031 | 0.029 | 0.024 | 0.024 | 0.081 | 0.043 | 0.087 | 0.058 | 0.087 | 0.029 | 0.062 | 0.042 | | |

(a)

| | 1 | 2 | 3 | 4 | 5 | 6 | 7 | 8 | 9 | 10 | 11 | 12 | 13 | 14 | 15 | 16 | | |
|------------------------|-------|-------|-------|-------|-------|-------|-------|-------|-------|-------|-------|-------|-------|-------|-------|-------|------|----|
| $S_{Sunny} M_{Sunny}$ | 5.014 | 5.018 | 5.066 | 4.951 | 5.072 | 5.036 | 5.023 | 5.079 | 5.329 | 5.384 | 5.166 | 5.136 | 5.174 | 5.136 | 4.159 | 4.173 | Mean | SD |
| $S_{Sunny} M_{Cloudy}$ | 5.069 | 5.074 | 5.174 | 4.969 | 5.076 | 5.062 | 5.097 | 5.112 | 5.234 | 5.32 | 5.162 | 5.128 | 5.214 | 5.196 | 4.177 | 4.183 | | |
| Difference | 0.055 | 0.056 | 0.108 | 0.018 | 0.004 | 0.026 | 0.074 | 0.033 | 0.095 | 0.064 | 0.004 | 0.008 | 0.040 | 0.060 | 0.018 | 0.010 | | |

(b)

The results show that in both cases (experienced vs. inexperienced), the mean errors are smaller for AIM, with 0.101cm against the 0.132cm of CM for the inexperienced case, and 0.126cm against 0.136cm for the experienced case. The same holds for the standard deviations, with 0.101cm for AIM against 0.150cm for CM in the inexperienced case, and 0.097cm for AIM against 0.139cm for CM in the experienced case. A larger standard deviation implies that it is more probable for AIM to have errors closer to the (smaller) mean. The results also show another interesting fact: the AIM error decreases for inexperienced operators, while the CM is maintained. These results prove, at least empirically, not only that our method is not affected by the experience level of the operator (and even improves slightly), but it is equivalent (slightly better) to the manual caliper method.

To conclude we presents a more detailed analysis of the outliers that produce the higher standard deviation of the CM method. For that we computed a histogram that counts the number of errors that each method presents on each diameter value. For simplicity we do not show the full histogram but instead highlight some outstanding facts. First we note that of all 840 cases, 62.2% of the CM measurements are smaller than the maximum mean 0.136cm, while AIM has 7.2% more cases within that range, i.e., 69.4%. Also, all the cases of the AIM method are smaller than 0.62cm, while only 98.6% of the CM measurements fall within that interval, with the remaining 1.4% reaching errors of up to 1.8cm. The 1.4% of 840 represents 12 measurements, which cannot be overlooked easily, and whose most probable cause is human error due to operator carelessness or fatigue.

Luminosity conditions experiment

The results for the luminosity conditions experiment are shown in Table 3 (in centimeters). The Table shows the comparison of the two cloudy cases $S_{cloudy} | M_{sunny}$ vs. $S_{cloudy} | M_{cloudy}$ (Table 3-a on top) and the comparison of the two sunny cases $S_{sunny} | M_{cloudy}$ vs. $S_{sunny} | M_{sunny}$ (Table 3-b on the bottom), for each of the 16 images, together with mean and standard deviation over the 16 images on the right. Both cases show a mean of approximately 0.04cm, a small discrepancy considering the errors of AIM (as shown in the previous experiment) are approximately 0.10cm. Therefore, we can conclude that, at least empirically, the segmentation algorithm is robust to changes in luminosity caused by cloudy skies. This justifies using a single, mixed luminosity GMM model for both luminosity conditions, as it was the case for the first experiment.

CONCLUSIONS

This paper has presented a high-precision and low-cost method based on Computer Vision for autonomous measurement of trunk diameter on grapevines from images acquired with a compact digital camera. This method is an important contribution in the field of autonomous sensing of complex variables in Precision Agriculture. In practice, generally, the trunk diameter is measured manually using Vernier calipers. This method involves human errors that can occur during measurement campaigns due to fatigue, haste or carelessness. There are several studies that address the problem of automating the measurement of trunk diameter trees. However, these solutions are not optimal: some are low cost but low precision (or equivalently high failing rate), and others are high precision but high cost. The experimental analysis for our method shows that it is more accurate than the manual method based on caliber, mainly because it is more robust to human error. An important advantage over other authors named in this work, is that the technology required to implement this method is cheap and probably any agronomist already has some of the main elements: a standard desktop computer and a low-resolution digital camera (3 megapixels). In addition, our method has two advantages over the manual method: avoid mistakes I, II, and IV, summarized in Table 2; and eliminates the qualifications of the operator as a factor of influence in results, i.e., it requires people with little or no knowledge and experience in agronomy experiments.

It is worth noting some open problems around the method proposed in this paper. Our method is still prone to error III of Table 2, since plants are not identified autonomously, still requiring a human to associate a photo ID with the plant. This is not difficult to automate however. For example, one solution is to include QR codes (28, 29) in the scene to identify automatically the plant of the image. This approach has been omitted in this work. In addition, automation of the measuring process such as trunk diameter makes it amenable to further automation. On one hand it may be embedded in an unmanned (air or land) vehicle that autonomously navigates the field taking measurements. On the other hand, it may be embedded in an information system for the management of experiment

campaigns that integrates the workflow for the whole agronomic experiment. Such a system could incorporate all the benefits of current technologies such as mobile photography and computing, GPS positioning, databases, web-based interfaces, and more (34, 38). This proposal is beyond the scope of this work. However, some members of our laboratory are working on a full report of this framework, including automated matching of plant and image. Finally, with the setting presented in this work, the errors incurred by the GMM algorithm are given only over a *corrupted zone*, corresponding to edges of the spade pads in the images. In Figure 2-c the error by corrupted zone is approximately 9 pixels corresponding to 0.9mm, but this value can vary depending of the images. Such error is caused by 3 main sources: imperfections of materials used in spade pads of the clamp; presence of high brightness over the edges of spade pads; information loss due to JPEG compression algorithm. Thus, our approach may greatly benefit by simple technical improvements such: smaller and easily manipulable clamp; possibility to include multiple clamps in the same image; and better materials for the spade pads that better resists wear and tear, thus reducing segmentation errors.

BIBLIOGRAPHY

1. Antuniassi, U. R.; Velini, E. D.; and Nogueira, H. C. 2004. Soil and weed survey for spatially variable herbicide application on railways. *Precision Agriculture*. 5:27–39.
2. Arnó Satorra, J.; Martínez Casasnovas, J. A.; Ribes Dasi, M.; and Rosell Polo, J. R. 2009. Review. Precision Viticulture. Research topics, challenges and opportunities in site-specific vineyard management. *Spanish Journal of Agricultural Research*. 7:779–790.
3. Bartelink, H. H. 1997. Allometric relationships for biomass and leaf area of beech (*Fagus sylvatica* L.). In *Annales des Sciences Forestieres*. EDP Sciences. 54:39–50.
4. Bishop, C. M. 2009. Pattern recognition and machine learning. Springer.
5. Blackmore, S.; and Robert, P. C. 2003. Precision farming: a dynamic process. In *Proceedings of the 6th International Conference on Precision Agriculture and Other Precision Resources Management*. Minneapolis, MN, USA. 84–104.
6. Bramley, R. G. V. 2009. Lessons from nearly 20 years of Precision Agriculture research, development, and adoption as a guide to its appropriate application. *Crop and Pasture Science*. 60:197–217.
7. Bramley, R. G. V.; and Lamb, D. W. 2003. Making sense of vineyard variability in Australia. In *Proc. Internat. Symp. on Precision Viticulture, Ninth Latin American Congr. on Viticulture and Oenology*. 35–54.
8. Bramley, R. G. V.; Proffitt, A. P. B.; Hinze, C. J.; Pearse, B.; Hamilton, R. P.; and STAFFORD, J. 2005. Generating benefits from Precision Viticulture through selective harvesting. In *Proc V ECPA-Eur Conf on Precision Agriculture*. Uppsala, Sweden. 8–11.
9. Brunelli, R. 2009. Template Matching Techniques in Computer Vision: Theory and Practice. Wiley.
10. Castelan-Estrada, M.; Vivin, P.; and Gaudillière, J. P. 2002. Allometric Relationships to Estimate Seasonal Above-ground Vegetative and Reproductive Biomass of *Vitis vinifera* L. *Annals of Botany*. 89:401–408.
11. Causton, D. R. 1985. Biometrical, structural and physiological relationships among tree parts. Attributes of trees as crop plants. Edited by MGR Cannel and JE Jackson. Titus Wilson & Son Ltd.. Cumbria, Great Britain. 137–159.
12. Chapman, C. A.; Chapman, L. J.; Wangham, R.; Hunt, K.; Gebo, D.; and Gardner, L. 1992. Estimators of fruit abundance of tropical trees. *Biotropica*. 527–531.
13. Cheng, H. D.; Jiang, X.; Sun, Y.; and Wang, J. 2001. Color image segmentation: advances and prospects. *Pattern recognition*. 34:2259–2281.
14. Chen, Y. R.; Chao, K.; and Kim, M. S. 2002. Machine vision technology for agricultural applications. *Computers and Electronics in Agriculture*. 36:173–191.
15. Cook, S. E.; and Bramley, R. G. V. 1998. Precision agriculture—opportunities, benefits and pitfalls of site-specific crop management in Australia. *Animal Production Science*. 38:753–763.
16. Cressie, N. 1990. The origins of kriging. *Mathematical Geology*. 22:239–252.
17. Doppelmanna, K. J.; and Berliner, P. R. 2000. Biometric relationships and growth of pruned and non-pruned *Acacia saligna* under runoff irrigation in northern Kenya. *Forest Ecology and Management*. 126:349–359.
18. Hastie, T.; Tibshirani, R.; and Friedman, J. H. 2009. The Elements of Statistical Learning: Data Mining, Inference, and Prediction. Springer.
19. Hemming, J.; and Rath, T. 2001. Computer-Vision-based Weed Identification under Field Conditions using Controlled Lighting. *Journal of Agricultural Engineering Research*. 78:233–243.
20. Jain, R.; Kasturi, R.; and Schunck, B. G. 1995. Machine vision. McGraw-Hill New York.

21. Jimenez, A.; Ceres, R.; Pons, J.; and others. 2000. A survey of computer vision methods for locating fruit on trees. *Transactions of the ASAE-American Society of Agricultural Engineers*. 43:1911–1920.
22. Jutila, J.; Kannas, K.; and Visala, A. 2007. Tree measurement in forest by 2D laser scanning. In *International Symposium on Computational Intelligence in Robotics and Automation, CIRA 2007*. Jacksonville, Florida, U.S.A: IEEE. 491–496.
23. Kan, J.; Li, W.; and Sun, R. 2008. Automatic measurement of trunk and branch diameter of standing trees based on computer vision. In *3rd IEEE Conference on Industrial Electronics and Applications, ICIEA 2008*. Singapore, Singapore: IEEE. 995–998.
24. Ketterings, Q. M.; Coe, R.; van Noordwijk, M.; Ambagau, Y.; and Palm, C. A. 2001. Reducing uncertainty in the use of allometric biomass equations for predicting above-ground tree biomass in mixed secondary forests. *Forest Ecology and management*. 146:199–209.
25. Kurtulmus, F.; Lee, W. S.; and Vardar, A. Immature peach detection in colour images acquired in natural illumination conditions using statistical classifiers and neural network. *Precision Agriculture*. 1–23.
26. Lee, W.; Slaughter, D.; and Giles, D. 1999. Robotic weed control system for tomatoes. *Precision Agriculture*. 1:95–113.
27. Li, Q.; Wang, M.; and Gu, W. 2002. Computer vision based system for apple surface defect detection. *Computers and electronics in agriculture*. 36:215–223.
28. Liu, Y.-C. 2013. Conceptual Design of Mobile Data Collection System for Traceability in Agriculture. *Advanced Science Letters*. 19:2947–2951.
29. Liu, Y.-C.; Gao, H.; and Zhang, X. 2012. Development and Application of Mobile Traceability Data Construction for Agriculture. In *8th Asian Conference for Information Technology in Agriculture and World Conference on Computer in Agriculture*. Taipei City, Taiwan.
30. Lott, J. E.; Howard, S. B.; Black, C. R.; and Ong, C. K. 2000. Allometric estimation of above-ground biomass and leaf area in managed *Grevillea robusta*. *Agroforestry Systems*. 49:1–15.
31. Lucchese, L.; and Mitra, S. K. 2001. Color image segmentation: A state-of-the-art survey. *Proceedings of the Indian National Science Academy (INSA-A)*. Delhi, Indian: Natl Sci Acad. 67:207–221.
32. MacAdam, J. W. 2013. *Structure and Function of Plants*. John Wiley & Sons.
33. Manh, A. G.; Rabatel, G.; Assemat, L.; and Aldon, M. J. 2001. AE–Automation and Emerging Technologies:: Weed Leaf Image Segmentation by Deformable Templates. *Journal of Agricultural Engineering Research*. 80:139–146.
34. McBratney, A.; Whelan, B.; Ancev, T.; and Bouma, J. 2005. Future directions of precision agriculture. *Precision Agriculture*. 6:7–23.
35. McCarthy, C.; Hancock, N.; and Raine, S. R. 2010. Applied machine vision of plants: a review with implications for field deployment in automated farming operations. *Intelligent Service Robotics*. 3:209–217.
36. McLachlan, G. J.; and Krishnan, T. 1997. *The EM algorithm and extensions*. Wiley New York.
37. Meyer, G. E.; and Neto, J. C. 2008. Verification of color vegetation indices for automated crop imaging applications. *Computers and Electronics in Agriculture*. 63:282–293.
38. Nikkilä, R.; Seilonen, I.; and Koskinen, K. 2010. Software architecture for farm management information systems in precision agriculture. *Computers and electronics in agriculture*. 70:328–336.
39. Niklas, K. J. 1994. *Plant Allometry: The Scaling of Form and Process*. University of Chicago Press.
40. Niklas, K. J. 1995. Size-dependent allometry of tree height, diameter and trunk-taper. *Annals of botany*. 75:217–227.
41. Omasa, K.; Hosoi, F.; Uenishi, T. M.; Shimizu, Y.; and Akiyama, Y. 2008. Three-dimensional modeling of an urban park and trees by combined airborne and portable on-ground scanning LIDAR remote sensing. *Environmental Modeling & Assessment*. 13:473–481.
42. Pajares, G.; Tellaeche, A.; BurgosArtizzu, X.-P.; and Ribeiro, A. 2007. Design of a computer vision system for a differential spraying operation in precision agriculture using Hebbian learning. *IET Computer Vision*. 1:93–99.
43. Pérez, D. S.; and Bromberg, F. 2012. Segmentación de imágenes en viñedos para la medición autónoma de variables vitícolas. In *XVIII Congreso Argentino de Ciencias de la Computación*.
44. Rodríguez-Pulido, F. J.; Ferrer-Gallego, R.; Lourdes González-Miret, M.; Rivas-Gonzalo, J. C.; Escribano-Bailón, M. T.; and Heredia, F. J. 2012. Preliminary study to determine the phenolic maturity stage of grape seeds by computer vision. *Analytica Chimica Acta*. 732:78–82.

45. Schumann, A. W. 2006. Nutrient management zones for citrus based on variation in soil properties and tree performance. *Precision Agriculture*. 7:45–63.
46. Shapiro, L.; and Stockman, G. 2001. *Computer Vision*. Prentice Hall.
47. Sogaard, H. T. 2005. Weed classification by active shape models. *Biosystems Engineering*. 91:271–281.
48. Szeliski, R. 2010. *Computer Vision: Algorithms and Applications*. Springer.
49. Tellaeche, A.; BurgosArtizzu, X. P.; Pajares, G.; Ribeiro, A.; and Fernández-Quintanilla, C. 2008. A new vision-based approach to differential spraying in precision agriculture. *Computers and Electronics in Agriculture*. 60:144–155.
50. Tetuko, J.; Tateishi, R.; and Wikantika, K. 2001. A method to estimate tree trunk diameter and its application to discriminate Java-Indonesia tropical forests. *International Journal of Remote Sensing*. 22:177–183.
51. Thamrin, N. M.; Arshad, N. H. M.; Adnan, R.; Sam, R.; Razak, N. A.; Misnan, M. F.; and Mahmud, S. F. 2013. Tree diameter measurement using single infrared sensor for non-stationary vehicle context in agriculture field. In 4th Control and System Graduate Research Colloquium (ICSGRC). Shah Alam, Malaysia: IEEE. 38–42.
52. Vann, D. R.; Palmiotto, P. A.; and Richard Strimbeck, G. 1998. Allometric equations for two South American conifers: test of a non-destructive method. *Forest Ecology and Management*. 106:55–71.
53. Zeng, Q.; Liu, C.; Miao, Y.; Fei, S.; and Wang, S. 2008. A machine vision system for continuous field measurement of grape fruit diameter. In 2th International Symposium on Intelligent Information Technology Application. Shanghai, China: IEEE. 2:1064–1068.
54. Zúniga, A.; Mora, M.; Oyarce, M.; and Fredes, C. 2013. Estimation of Grape Maturity Based on Neural Networks. In International Conference of The Chilean Computer Science Society. Temuco, Chile.

ACKNOWLEDGMENTS

This work was funded by the scholarship program of the *National Technological University* (UTN) and the *National Fund for Scientific and Technological Promotion* (FONCyT) of Argentina. We thank the *Department of Plant Physiology*, Faculty of Agricultural Sciences, UNCuyo, for offering their vineyards to capture the images used in this work.

APPENDIX A: Image Segmentation

Image Segmentation is to partition an image into a set of non-overlapping regions, which have a consistent semantics about a particular application (46). Ideally are expected that regions represent an object or parts of it. The extracting process from domain of one or more image regions, which satisfy a uniformity or homogeneity criterion, is mainly based on the characteristics derived from color space. This process can be enhanced by some additional knowledge about the objects in the scene, such as geometric and optical properties (31). Formally, the segmentation process is defined as a method to partitioning an image I in regions R_k , with $k=1, \dots, K$, such that each region R_k is a candidate object (20):

Definition 1. A region is a subset of pixels in an image I .

Definition 2. Segmentation is the grouping of pixels into regions, such that:

- The regions R_k form a partition, i.e., they encompass the whole image and do not overlap each other.
- Each region R_k satisfies *uniformity criteria* (all pixels in the region have one or more common properties).
- The pixels belonging to adjacent regions, when taken together, do not satisfy the *uniformity criterion*.

With these definitions, the *uniformity criterion* is the most important element of this model, and can be as simple as uniformity in the color intensity of the pixels, while generally is more complex, often depending on the application.

APPENDIX B: Color Spaces

Generally, the pictures taken with conventional digital cameras are in the RGB color space, which means that the color of a pixel is represented as a point in 3-dimensional space comprising the intensities of the red (R), green (G), and blue (B) component (20, 48). From combination of these intensities any color can be represented. RGB is suitable for color display (television systems and digital cameras), but not usually suitable for task analysis and image segmentation. This is due to the high correlation between R, G, and B, i.e., if you change the intensity or brightness of a pixel, the three components change accordingly. Moreover, color measurement in the RGB space not represents color differences in a uniform scale; therefore, it is impossible to evaluate the similarity of two colors from the distance in the RGB space (13). However, the RGB representation can be derived other color spaces by using linear or non-linear transformations. Color spaces such as RGB, HSI, HSV, LUV, LAB, etc., are used in image segmentation, but none of them is superior to the other in all kinds of images, and often depends on the problem (20, 48). In this paper, the original images were converted from RGB to LUV (*L=luminescence*, *U=saturation*, *V=hue angle*). LUV separates the color information of an image from intensity information. Color information is represented by a tone (V) and saturation values (U), while the intensity, which describes the brightness of an image is determined by the amount of light (L). Thus LUV has several advantages over RGB: we can control the color information and the intensity of a way simpler and independent; we allows to directly compare two colors based on geometric separation in color space, therefore, is especially efficient to the measurement of small differences in color; and we reduces dimensionality problem, since in this work only the color information (UV components) is used, discarding intensity information (component L) (13, 20, 48).